LAWRENCE
LIVERMORE
NATIONAL
LABORATORY

LLNL-CONF-424403

An Experimental and Kinetic Modeling Study of Methyl Decanoate Combustion

S. M. Sarathy, M. J. Thomson, W. J. Pitz, T. Lu

February 23, 2010

Combustion Institute Western States Spring Technical Meeting
Boulder, CO, United States
March 22, 2010 through March 24, 2010

Disclaimer

An Experimental and Kinetic Modeling Study of Methyl Decanoate Combustion

S.M. Sarathy[a], M.J. Thomson[b], W.J. Pitz[a], T. Lu[c]

[a] *Physical and Life Sciences Directorate, Lawrence Livermore National Laboratory*
[b] *Department of Mechanical and Industrial Engineering, University of Toronto*
[c] *Department of Mechanical Engineering, University of Connecticut*

Abstract

Biodiesel is typically a mixture of long chain fatty acid methyl esters for use in compression ignition engines. Improving biofuel engine performance requires understanding its fundamental combustion properties and the pathways of combustion. This research study presents new combustion data for methyl decanoate in an opposed-flow diffusion flame. An improved detailed chemical kinetic model for methyl decanoate combustion is developed, which serves as the basis for deriving a skeletal mechanism via the direct relation graph method. The novel skeletal mechanism consists of 648 species and 2998 reactions. This mechanism well predicts the methyl decanoate opposed-flow diffusion flame data. The results from the flame simulations indicate that methyl decanoate is consumed via abstraction of hydrogen atoms to produce fuel radicals, which lead to the production of alkenes. The ester moiety in methyl decanoate leads to the formation of low molecular weight oxygenated compounds such as carbon monoxide, formaldehyde, and ketene.

Key words: methyl decanoate, skeletal mechanism, biodiesel, combustion, chemical kinetic model

1. Introduction

Real biodiesel is a complex mixture of fatty acid methyl esters (FAME) with differing chain lengths and degrees of unsaturation, so it is much simpler to study the combustion chemistry of pure FAME. However, the numerous possible reaction pathways for long chain FAME would result in extremely large detailed chemical kinetic mechanisms. Such mechanisms are difficult to develop and computationally expensive to solve in even the simplest physical reactor models. Furthermore, conducting fundamental combustion experiments using long chain (i.e., high molecular weight) FAME is challenging because vaporisation is difficult.

In order to avoid the difficulties associated with long chain FAME, surrogate fuels with shorter chain lengths and known physical chemical properties are chosen for biodiesel combustion chemistry studies. Using surrogate fuels simplifies the chemical kinetic mechanism by reducing the number of possible chemical reactions, while still representing the role of the molecular structure in combustion (i.e., the role of the methyl ester moiety and the role of carbon-carbon double bonds). In addition, surrogates fuels are more volatile, and therefore easier to work with experimentally.

Figure 1 displays typical biodiesel FAME and several proposed surrogates. The surrogate fuels are structurally similar to actual biodiesel FAME, and all but one contain the ester moiety. The chain length and degree of unsaturation varies in the surrogate fuels, so the individual effects of each can be understood. The remainder of this introduction discusses the recent advances in the chemical kinetic modeling of FAME surrogate fuels. Particular attention is placed on the chemistry related effects of the ester moiety, carbon chain length, and carbon-carbon double bonds during combustion.

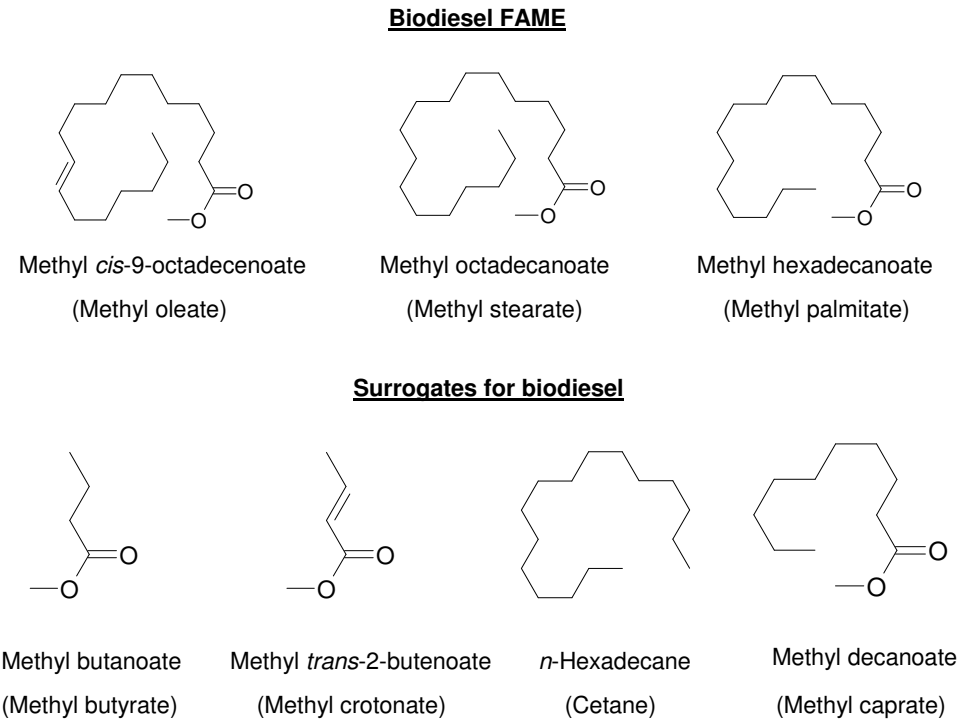

Figure 1: Biodiesel FAME and their surrogates

1.1. Mechanisms for Short Chain Methyl Esters

Fisher and coworkers [1] were the first to develop a detailed chemical kinetic for a biodiesel surrogate, methyl butanoate (MB). While the mechanism was complete, the authors were unable to robustly validate the model due to limited experimental data on MB combustion. Gail et al. [2] were the first to extensively validate a slightly modified version of the Fisher mechanism for MB using experimental data from a jet stirred reactor (JSR), an opposed-flow diffusion flame, and a flow reactor. Recently, a number of studies have been conducted to further study the combustion of MB and validate chemical kinetic mechanisms [3–8]. In addition, theoretical studies have performed *ab initio* calculations of thermochemical properties [9–12] and kinetic rate parameters [8, 13, 14] for MB. Experimental and modeling studies have also been conducted on methyl *trans*-2-butenoate [15, 16] and ethyl propanoate [5, 17].

The various studies on MB and MC have revealed consistent conclusions. Firstly, quantum calculations of thermochemical properties suggest that small methyl esters are a good surrogate fuel for representing the thermochemistry of saturated long chain FAME. However, autoignition and low temperature experimental data indicate that MB does not exhibit cool flame and negative temperature coefficient (NTC) behaviour, which are significant characteristics of the longer chain FAME found in biodiesel. Vaughan et al. [18] and Hadjiali et al. [19] also found that the ignition delay time of MB did not match well with those of longer chain FAME. Therefore, due to its short chain length, MB, and other small esters, are not a suitable surrogate for understanding the low temperature reactivity and autoignition properties of biodiesel. However, blends of *n*-heptane plus MB have been used to simulate combustion in engines [20, 21].

1.2. Mechanisms for Long Chain Methyl Esters

Recently, the research focus has shifted to longer chain esters. Experimental and modeling studies of methyl hexanoate [22] and methyl heptanoate [23] in a JSR have been performed. Zhang et al. have presented motored engine experimental data of methyl heptanoate [24] and various C_9 FAME [25].

In an effort to study the longer chain FAMEs found in real biodiesel, Dagaut and coworkers [26] studied the oxidation of rapeseed oil methyl ester (RME) in a JSR at various temperatures and pressures. The authors proposed that a long chain alkane would be a suitable surrogate for RME since experimental data for *n*-hexadecane ($C_{16}H_{34}$) in the JSR at similar conditions indicated similar product species concentration profiles. A detailed chemical kinetic mechanism for *n*-hexadecane gave a good description of the RME experimental results, with a good agreement for RME reactivity and the relative importance of C_2-C_6 alkenes. The authors stated that the mechanism could be improved by including chemical kinetic pathways for the following: i. the ester moiety to reproduce the early CO_2 formation found in RME, and ii. carbon double bonds to reproduce large alkene production in RME attributed to unsaturated FAMEs.

1.3. Mechanisms for Methyl Decanoate

Methyl decanoate has been proposed as a much better surrogate for biodiesel due to the length of the alkyl chain. Studies by Vaughan et al. [18] and Szybist et al. [27] found that MD had similar ignition times and NTC behaviour to real biodiesel fuels. Herbinet et al. [28] developed a detailed chemical kinetic mechanism for MD consisting of 3012 species and 8820 reactions, and validated the mechanism against MD data in motored engine [27] and rapeseed oil methyl ester oxidation data in a JSR [26]. The MD mechanism is capable of reproducing the early CO_2 formation observed for RME in the JSR, a behaviour that the *n*-hexadecane model by Dagaut et al. [26] could not reproduce. The chemical kinetic mechanism reveals that low temperature formation of CO_2 comes directly from the presence of the ester group, and since CO is not formed directly, the soot reducing efficiency of the fuel-bound oxygen is not maximized. The mechanism is unable to reproduce large alkene production in RME because MD is too small, and it does not contain

the double bonds which lead to alkene formation. In addition, the large size of this mechanism requires a robust numerical solver and enormous computing power when attempting to model combustion in some configurations, such as laminar flames.

The aforementioned detailed MD chemical kinetic mechanism is limited in its applicability due to the large number of species and reactions. In addition, the chemical stiffness, which is characterized by dramatic differences between species and reaction time scales, is significant for the large molecules in the detailed mechanism [29]. Using this mechanism in a zero-dimensional simulation (i.e., JSR) is computationally expensive, and henceforth a one-dimensional simulation (i.e., opposed-flow diffusion flame) is impractical. To overcome these problems, Seshadri and coworkers used the direct relation graph (DRG) method to reduce the detailed mechanism into a skeletal mechanism consisting of 713 elementary reactions and 125 species [30]. The skeletal mechanism was capable of predicting experimental extinction and ignition of MD in an opposed-flow diffusion flame. A large number of low temperature chemical reactions in the original mechanism were discarded during the reduction, indicating that low temperature chemistry is of minor importance in an opposed-flow diffusion flame.

2. Research Motivation

The goal of this study is to develop a chemical kinetic mechanism for MD combustion in a flame. The existing detailed MD mechanism by Herbinet et al. [28] and the skeletal mechanism by Seshadri et al. [30] have not been validated against species profiles in an MD flame because such experiments have not been performed. This study presents new experimental temperature and species concentration profiles for an MD opposed-flow diffusion flame, and uses this data to validate an improved skeletal mechanism for MD combustion.

3. Experimental Methods

A detailed explanation of the experimental opposed-flow diffusion flame and corresponding sampling setup has been described by Sarathy et al. [31]. A fuel mixture of 98.2% N_2 and 1.8% fuel (99% pure MD) is fed through the bottom port at a mass flux of 0.0142 g/cm^2-sec, while an oxidizer mixture of 42.25% O_2 and 57.75% N_2 is fed through the top port at a mass flux of 0.0137 g/cm^2-sec. At these plug flow conditions, the Reynold's Number is in the laminar flow regime (i.e. $Re < 400$), the flame is on the fuel side of the stagnation plane, and the fuel side strain rate is approximately 31 s^{-1}. An ultrasonic atomizer sprays the liquid fuel into a stream of N_2 gas. The temperatures of the gases exiting the top and bottom burner ports were 420 K and 400K , respectively.

Analytical techniques used to measure the species in the sample included: non-dispersive infrared detection (NDIR) for CO and CO_2; gas chromatography/flame ionization detection (GC/FID) with an HP-Al/S

PLOT column for C_1 to C_5 hydrocarbons; and GC/FID equipped with a methanizer (i.e., Ni catalyst) and Poraplot-U column for oxygenated hydrocarbons such as acetaldehyde/ethenol, formaldehyde, and acrolein. The precision of species measurements is estimated to be ± 15%. Temperature measurements were obtained using a 254 μm diameter wire R-type thermocouple (Pt-Pt/13% Rh) in an apparatus similar to that used by McEnally et al. [32]. The measured temperatures were corrected for radiation losses.

4. Computational Methods

The kinetic modeling for MD oxidation in the opposed-flow diffusion flame was performed using the OPPDIF code within the CHEMKIN modeling package [33]. The inputs to each simulation include a detailed chemical kinetic reaction mechanism, a dataset of thermochemical properties, and a dataset of transport properties.

4.1. Chemical Kinetic Mechanism

The chemical kinetic mechanism developed here is an extension of previously published detailed and skeletal mechanisms for MD. The large size of Herbinet et. al's [28] detailed mechanism makes it impractical for use in the one-dimensional flame code (i.e., OPPDIF), and we found that the skeletal mechanism proposed by Seshadri et al. [30] does not contain enough species and reactions to accurately predict species concentration profiles in the opposed-flow diffusion flame. Therefore, the present study develops an intermediate size mechanism, which balances computational performance and chemical fidelity. Initially, several modifications were made to the detailed chemical kinetic mechanism to better represent MD combustion, and then this modified mechanism was reduced using the DRG method.

4.1.1. Modified Detailed Chemical Kinetic Mechanism

Herbinet et al.'s detailed chemical kinetic mechanism includes low temperature chemistry to simulate fuel ignition and NTC behaviour, as well as intermediate and high temperature chemistry to simulate fuel combustion and product species formation. Low temperature chemistry is not addressed in the present study because the consumption of fuel in an opposed-flow diffusion flame is dominated by high temperature chemical reactions. Therefore, the high temperature part of the detailed methyl decanoate mechanism and the corresponding modifications are discussed here.

For the most part, the high temperature consumption of MD proceeds similarly to a straight-chain alkane. The decomposition is driven by unimolecular decomposition and H-atom abstraction reactions leading to alkyl and alkyl-ester radicals. These radicals then react via isomerization, decomposition (e.g., *beta*-scission) and bimolecular reactions with O_2.

The unimolecular decomposition reactions were written in the reverse radical-radical recombination direction and the rate for the decomposition direction was calculated from thermochemistry via microscopic

reversibility. The rates for unimolecular decomposition reactions were based on a previous mechanism for MB by Fisher et al. [1]. H-atom abstraction from MD and other hydrocarbon molecules were included for reactions with radicals (e.g., H, CH_3, O, OH, etc.), and the rates were determined based on typical hydrocarbon C-H bond energies for primary, secondary, and tertiary H atoms. The reaction rates for the two H atoms bonded to the carbon atoms adjacent to the carbonyl group were based on the mechanism for MB by Fisher et al. The reader is referred to the original article [28] for further details on the detailed mechanism.

The following list of modifications were made to better represent the combustion of MD in the opposed-flow diffusion flame:

- Herbinet et al. [34] reported an error in their mechanism [28] for the activation energy for H-atom abstractions reactions by OH from secondary C-H bonds, so this was corrected in the present mechanism.

- The recombination rate of 1-octene (C_8H_{16}) and the ME2J radical to form the MD4J radical (i.e., reverse of the decomposition of the MD4J radical, as shown Figure 2) was changed to

$$8.80x10^3 \cdot T^{2.48} \exp\left(\frac{-6130\frac{cal}{mol}}{RT}\right) \frac{cm^3}{mol \cdot s}$$

to make it consistent with rates of analogous reactions for the MB5J, MB6J, MB7J, etc. radicals.

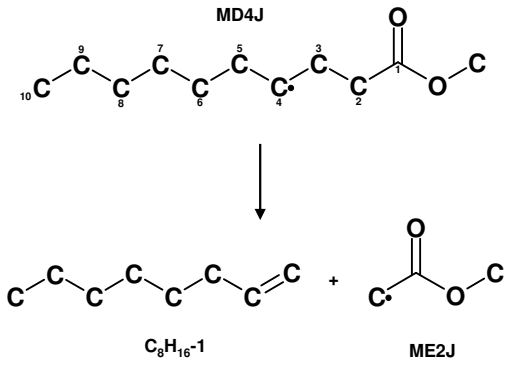

Figure 2: Decomposition of the MD4J radical to 1-octene (C_8H_{16}) and the ME2J radical

- The recombination rate of methyl 2-propenoate (MP2D) and the 1-heptyl radical (C_7H_{15}) to form the MD2J radical (i.e., reverse of the decomposition of the MD2J, as shown Figure 3) was changed to

$$1.76x10^4 \cdot T^{2.48} \exp\left(\frac{-8130\frac{cal}{mol}}{RT}\right) \frac{cm^3}{mol \cdot s}$$

based on the rate expression given by Curran et al. [35] for the recombination of propene (C_3H_6) and the methyl radical (CH_3) to form the 2-butyl radical (sC_4H_9) (i.e., reverse of the decomposition of the sC4H9). Curran's estimate was modified by 2 kcal/mol to account for resonance stabilization effects of the carbonyl group in MD2J [4].

- Hydrogen atoms bonded to the alpha carbon (see Figure 4) have BDEs similar to tertiary C-H bonds in alkanes [4]. Therefore, H atom abstraction rates by the radicals H, OH, CH_3, CH_3O, and HO_2 were changed to analagous rates for tertiary H atom abstraction in isobutane (iC_4H_{10}). The rates for isobutane from Healy et al. [36] were multiplied by 2 to account for greater number of H atoms in the MD2J radical.

Figure 5 displays JSR simulations using various FAME and alkane mechanisms at ϕ=1.0, P=1013 kPa, τ=1 s, 0.1% fuel mole fraction. *n*-Decane simulations [37] and experimental data [38] match well, with both

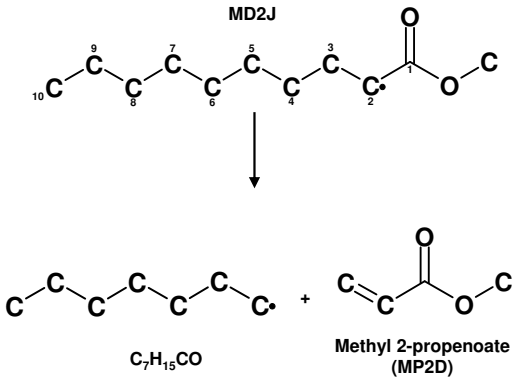

Figure 3: Decomposition of the MD2J to methyl 2-propenoate (MP2D) and the C_7H_{15} radical

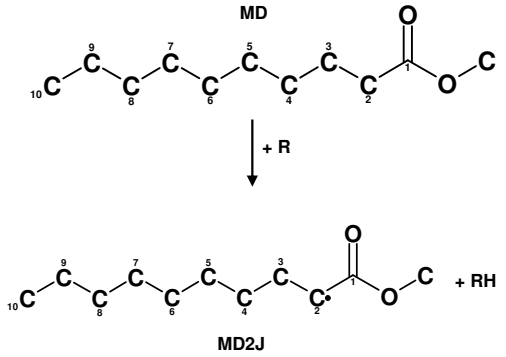

Figure 4: Abstraction of H atoms from the methoxy carbon atom by a reactive radical species (R)

showing cool flame reactivity in the range of 600-800 K. Simulations using Dooley's MB mechanism [4] and Seshadri's skeletal MD mechanism [30] indicate that these models lack cool flame behaviour, and therefore they are not suitable for modeling real biodiesel low temperature chemistry.

It is observed that Herbinet's detailed MD mechanism [28] displays cool flame reactivity, but when compared to simulations for *n*-decane [37], the MD model appears to overpredict the fuel's reactivity. One would expect the reactivity of MD and *n*-decane in the JSR to be similar since both contain C_{10} alkyl chains, and shock tube studies also indicate that their reactivity is similar [28]. This model behavior was due to incorrect activation energies for H atom abstractions reactions by OH from secondary C-H bonds, as mentioned previously. After correcting these values, the modified detailed MD mechanism well predicts the reactivity of *n*-decane.

4.1.2. Skeletal Chemical Kinetic Mechanism

The modified detailed chemical kinetic mechanism with 3012 species and 8820 reactions is impractical for use in a one-dimensional flame code. Mechanism reduction methods are available to reduce the detailed mechanism's size and complexity. In this study, the DRG method is used to generate a skeletal version of

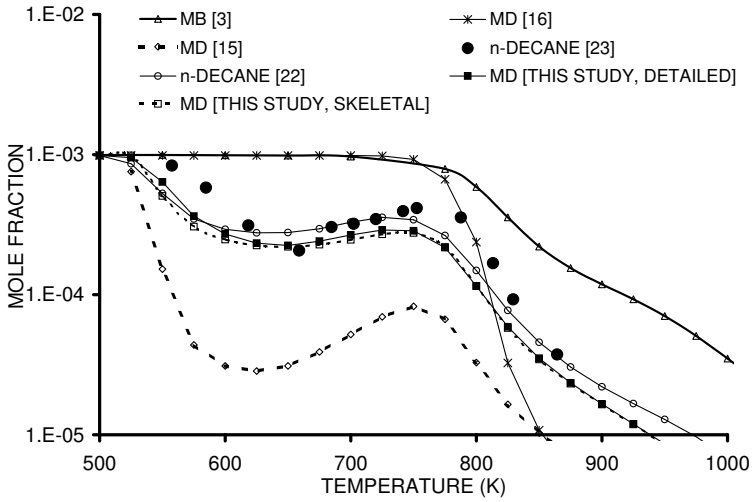

Figure 5: Computed profiles obtained from the oxidation of methyl decanoate, *n*-decane, and methyl butanoate in a JSR at ϕ=1.0, P=1013.25 kPa, τ=1 s, 0.1% fuel mole fraction.

the modified detailed MD mechanism discussed previously.

Seshadri et al. [30] used the DRG method to generate an MD skeletal mechanism consisting of 125 species and 713 elementary reactions. The DRG is a systematic algorithm used for eliminating unimportant species and reactions from a detailed mechanism. In this method a directed graph is used to detect all the species in the mechanism that are strongly coupled to the fuel and oxidizer [29]. The directed graph is generated using sampling points covering a wide range of temperatures, pressures, fuel-oxygen-nitrogen mixture fractions, and fluid mixing conditions, such that the couplings remain valid for combustion in various platforms (i.e., laminar flames, shock tubes, jet-stirred reactors, etc.). The DRG methodology and its applicability to various hydrocarbon mechanisms is available in the literature [39, 40].

Figure 6 compares the skeletal MD mechanism of Seshadri et al., the detailed MD mechanism by Herbinet et al. [28], and experimental data for RME in a JSR [26]. The 125 species mechanism by Seshadri et al. poorly predicts the concentrations of carbon dioxide, carbon monoxide, and methane, especially at lower temperatures. This indicates that the mechanism lacks chemical fidelity when compared to the detailed mechanism.

In order to improve the DRG method, the sample space was chosen as follows:

- combustion in a homogeneous gas phase plug flow reactor at 101.3 kPa and 1013 kPa, 900-1800 K, ϕ=0.25-2.0, with mixtures of both undiluted fuel and diluted fuel (i.e. 2% MD, 98% N_2) plus air. These

conditions were simulated using the SENKIN code in CHEMKIN

- combustion in a perfectly stirred reactor (PSR) at 101.3 kPa and 1013 kPa, 900-1500 K, ϕ=0.25-2.0, τ=0.0001-1 s, and mixtures of undiluted fuel plus air. These conditions were simulated using the PSR code in CHEMKIN.

The directed graph generated from the above sampling points was used to generate a skeletal mechanism consisting of 648 species and 2998 reactions. This skeletal mechanism accurately reproduces the low temperature reactivity predicted by the detailed mechanism, as shown in Figure 5. In addition, there is a good agreement between the new skeletal mechanism and Herbinet's detailed mechanism [28] for predicted species profiles of RME in the JSR, as shown in Figure 6. This indicates that the proposed skeletal mechanism is acceptable for modeling detailed chemical kinetic processes in the JSR. Furthermore, it is suitable replacement to the detailed mechanism for predicting the combustion properties of MD.

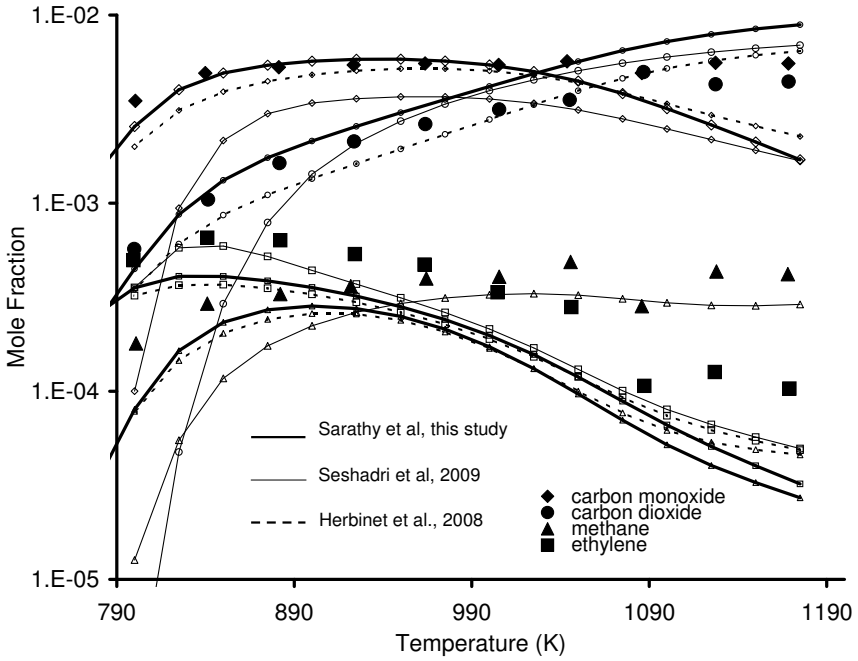

Figure 6: Comparison of MD mechanisms and experimental data for RME in a JSR at ϕ=1.0, P=101.325 kPa, τ=1.0 s [26].

4.2. Thermochemical Data

The thermochemical data for MD published by Herbinet et al. [28] was used in this study. The thermochemical properties for molecules and radicals were calculated using THERM [41], which is a software based on the group and bond additivity methods proposed by Benson [42]. THERM determines the thermochemical properties of a radical species by applying a bond dissociation (BD) group increment to a stable molecule which reflects the loss of an H atom from that species. The BD groups are based on specific

bond energies and difference in heat capacities and entropies for specific molecular classes [41]. For more accurate calculations, the user can modify BD group values for specific molecular classes based on *ab initio* thermochemical calculations, such as those by Sumathi and Green [43].

It was found that the BD groups used in the calculation of thermochemical properties for the radicals of methyl ethanoate (ME), ME2J and MEMJ, were inaccurate in the original work [28]. They were hence updated based on bond energies calculated by El-Nahas et al. [9]. The new thermochemical parameters make these molecules more stable and decrease their decomposition rates.

4.3. Transport Properties

This study builds upon the transport property database developed by Seshadri et al. [30] for the 125 species contained within their MD skeletal mechanism. The transport properties of species with no previously published data were determined as follows. Most of the transport parameters that needed to be determined were for stable C_2-C_{10} saturated and unsaturated methyl esters and their corresponding radicals. We assume that the transport properties are similar for saturated and unsaturated methyl esters of the same chain length, so we only performed calculations for saturated methyl esters and used the same values for their unsaturated counterparts. For methyl ester radical species, the transport properties of their stable counterpart were used.

For the stable saturated methyl ester species, this study used the correlations developed by Tee, Gotoh, and Stewart [44], as described by Wang and Frenklach [45], to calculate the Lennard-Jones collision diameter and potential well depth using the P_c, T_c, and T_b of the species. For C_2-C_6 methyl esters, these values were obtained from the NIST Chemistry WebBook [46], but the P_c, T_c values were not available for C_7-C_{10} methyl esters. However, a strong correlation exists between carbon chain length and P_c and T_c for C_3-C_6 methyl esters, as shown in Figure 7, so we extrapolated the P_c and T_c for larger methyl esters using a power law function.

Experimentally measured dipole moments were obtained from Mcclellan's text [47]. This property was available for C_3-C_6 methyl esters but not for C_7-C_{10} methyl esters. The molecular dipole moment is a vector property that can be determined for an unknown molecule using vector addition of known bond moments [48]. However, such a method requires detailed information of the geometry of molecular bonds and their electronegativities (i.e., polarity). The problem is simplified in the present study because experimentally measured dipole moments for saturated C_3-C_6 methyl esters fall in the range of 1.61-1.76 Debyes. This indicates that the molecular dipole moment is created by the ester moiety, which exhibits a strong polarity, and not the saturated alkyl chain, which is nonpolar. Therefore, a dipole moment of 1.70 Debyes was used for the C_7-C_{10} methyl esters.

Experimentally measured values for polarizability (α) in cubic Angstroms ($Å^3$) were obtained from the CRC Handbook of Chemistry and Physics [49]. The polarizability can also be determined using the empirical

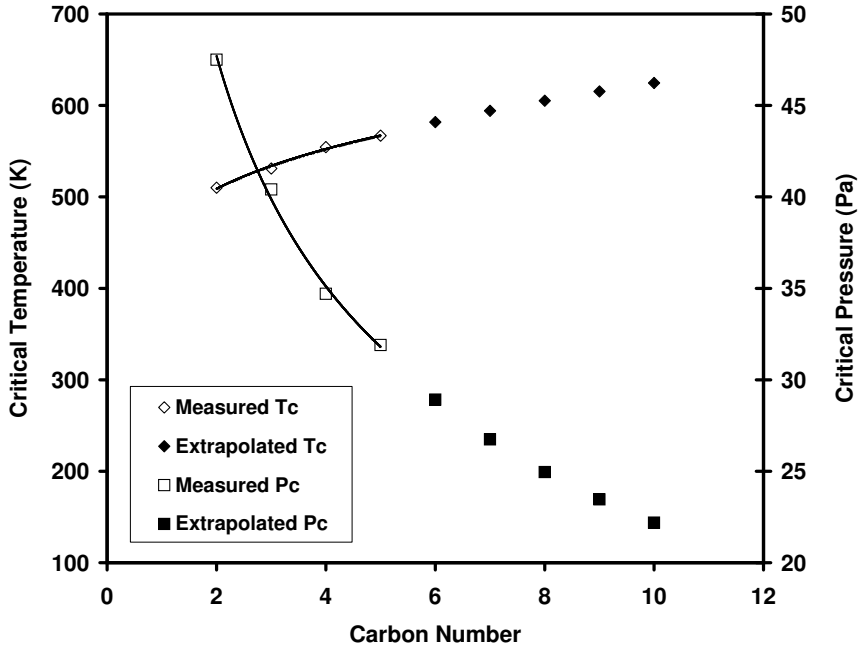

Figure 7: Critical pressure (P_c) and critical temperature (T_c) for C_2-C_{10} methyl esters.

relation proposed by Bosque and Sales [50], which allows estimation using the molecular formula (i.e., # of C, H, and O atoms), as shown in Equation 1. Table 1 presents experimentally and empirically determined polarizabilities for several FAME. The calculated values are within ±1% of the measured values for C_3-C_6 methyl esters, so a high degree of confidence accompanies the calculated polarizabilities for C_7-C_{10} methyl esters.

$$\alpha = 0.32 + 1.51 * \#C + 0.17 * \#H + 0.51 * \#O \tag{1}$$

5. Results and Discussion

5.1. Opposed-Flow Diffusion Flame

The proposed skeletal MD mechanism was validated against experimental data obtained in an MD opposed-flow diffusion flame. The opposed-flow diffusion flame allows the study of fuel oxidation in a non-premixed laminar flame environment. Concentration profiles for species were obtained by sampling the product gas at various points between the two burner ports and then analyzing it using a variety of analytical techniques. The measured species included methyl decanoate (MD), carbon monoxide (CO), carbon dioxide (CO_2), formaldehyde (CH_2O), methane (CH_4), acetylene (C_2H_2), ethylene (C_2H_4), ethane (C_2H_6), ketene

Table 1: Experimentally and Empirically Determined Polarizabilities (Å^3) for FAME

	Molecular Formula	Experimental [49]	Empirical [50]
Methyl ethanoate	$C_3H_6O_2$	6.94	6.89
Methyl propanoate	$C_4H_8O_2$	8.97	8.74
Methyl butanoate	$C_5H_{10}O_2$	10.41	10.59
Methyl pentanoate	$C_6H_{12}O_2$	-	12.44
Methyl hexanoate	$C_6H_{14}O_2$	-	14.29
Methyl heptanoate	$C_7H_{16}O_2$	-	16.14
Methyl octanoate	$C_8H_{18}O_2$	-	17.99
Methyl nonanoate	$C_9H_{20}O_2$	-	19.84
Methyl decanoate	$C_{10}H_{22}O_2$	-	21.69

(CH_2CO), propane (C_3H_8), propene (C_3H_6), propyne (pC_3H_4), 1-butene (1-C_4H_8), 1,3-butadiene (1,3-C_4H_6), 1-pentene (1-C_5H_{10}), 1-hexene (1-C_6H_{12}), 1-heptene (C_7H_{14}), and 1-octene (1-C_8H_{16}). A species profile was identified for C_2H_4O, but we are unable to determine if the compound is ethanal (i.e., acetaldehyde) (CH_3CHO) or ethenol (C_2H_3OH) since both have the same retention time on the GC column. In addition, ethenol rapidly tautomerizes to acetaldehyde upon contact with surfaces [51, 52], so we assume that the C_2H_4O measured in the GC is the combined concentration of acetaldehyde and ethenol in the flame. Species below the experimental limit of detection (LOD) (i.e., 5 ppm) included 1-butyne, *n*-butane, 2-butyne, *trans*-2-butene, *cis*-2-butene, pentane, hexane, propanal, 2-propenal (i.e., acrolein), 2-propanone (i.e., acetone), butanal, methyl 2-propenoate, methyl 3-butenoate, mehtyl 4-pentenoate, and methyl 5-hexenoate.

5.2. Temperature, Fuel, and Hydrocarbon Species

Figures 8 to 13 display the measured and predicted species and temperature profiles obtained in the opposed-flow diffusion flame. The experimental results (solid symbols) show that the MD concentration begins decreasing quickly at a distance of 5 mm from the fuel port. As the fuel is consumed, the CO and CO_2 concentrations begin rising. All of the MD is consumed at a distance of approximately 8.25 mm from the fuel port, which corresponds closely the visually observed flame front. Both the temperature and CO_2 concentrations reach their maximum at approximately 9.5 mm from the fuel port. Just before the flame front, at around 7.75 mm from the fuel port, the concentrations of hydrocarbon species reach their maximum. Besides CO and CO_2, the most abundant measured species are C_2H_4, C_2H_2, CH_4, and C_3H_6.

The model's prediction of temperature species profiles in the opposed-flow diffusion is shown in Figures 8. The model reproduces the experimentally measured temperature profile very well. The reactivity of MD is also well predicted by the model. The maximum concentration of CO_2 is underpredicted by by

approximately 0.3%, while the maximum concentration of CO is underpredicted by approximately 0.1%.

The model well reproduces the shape of the experimental profiles and the height and position of maximum measured concentrations. In the following discussion, the model's quantitative prediction is considered good if the predicted maximum mole fraction is within a factor 1.5 of the measured maximum mole fraction. The model performs well in predicting the maximum concentrations of CH_4, C_2H_6, C_3H_4, C_3H_6, 1-C_4H_8, C_8H_{16}, C_5H_{10}, C_6H_{12}, C_7H_{14}, CH2CO, and 1,3-C_4H_6. The model moderately underpredicts (i.e., 1.5-2 times) the maximum concentration of C_2H_4 and overpredicts the concentration of C_2H_2. Both model and the experimental data indicate that the concentration of 1-alkenes decreases with increasing carbon number.

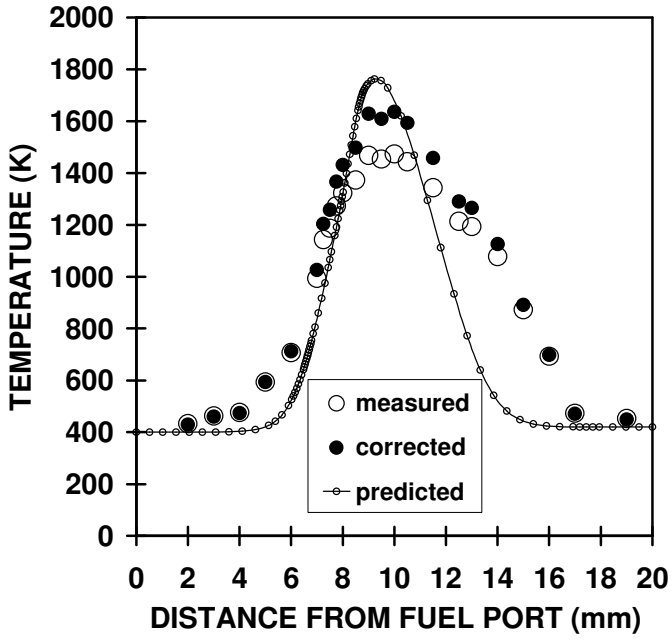

Figure 8: Experimental and computed temperature profiles obtained from the oxidation of MD in an atmospheric opposed-flow flame (1.8% MD, 42% O_2).

A reaction path analysis was performed for MD at 1033 K, the temperature at which approximately 50% of the fuel is consumed. Approximately 97% of the fuel is consumed via H atom abstraction by H atoms (58%), OH radicals (4%), and CH_3 radicals (28%). Abstraction is favoured for H atoms bonded to the α carbon (19%) and the other secondary carbons in the alkyl chain (10% each).

As shown in Figure 14, H-atom abstraction from the α carbon leads to the formation of the MD2J radical, which undergoes β-scission (99%) to form a 1-heptyl radical and methyl 2-propenoate. The 1-heptyl radical eventually leads to the formation of ethylene, 1-pentene, 1-butene, and the radicals C_3H_7 and C_2H_5, while the fate of methyl 2-propenoate is discussed in the next section. The measureable levels of ethylene, 1-pentene, and 1-butene in the flame experiments agree with this reaction path analysis.

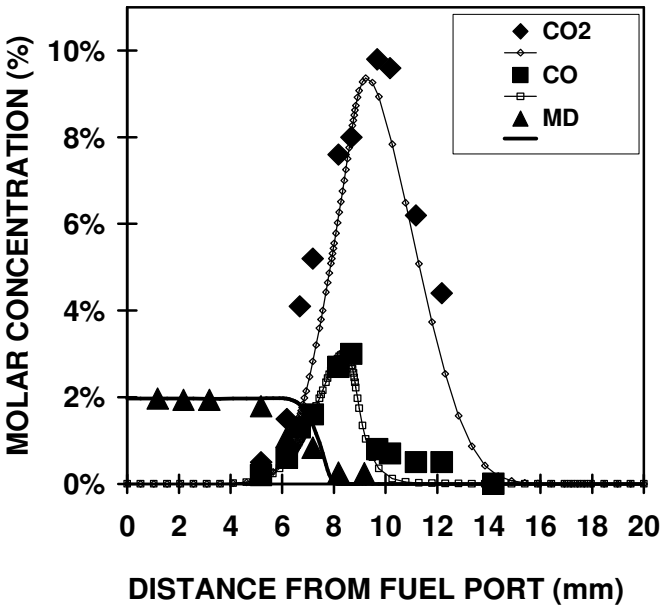

Figure 9: Experimental and computed species profiles obtained from the oxidation of MD in an atmospheric opposed-flow flame (1.8% MD, 42% O_2).

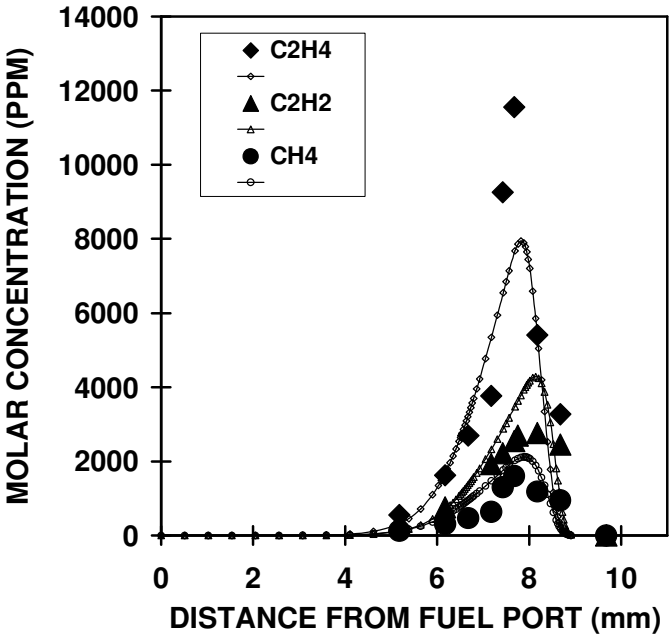

Figure 10: Experimental and computed species profiles obtained from the oxidation of MD in an atmospheric opposed-flow flame (1.8% MD, 42% O_2).

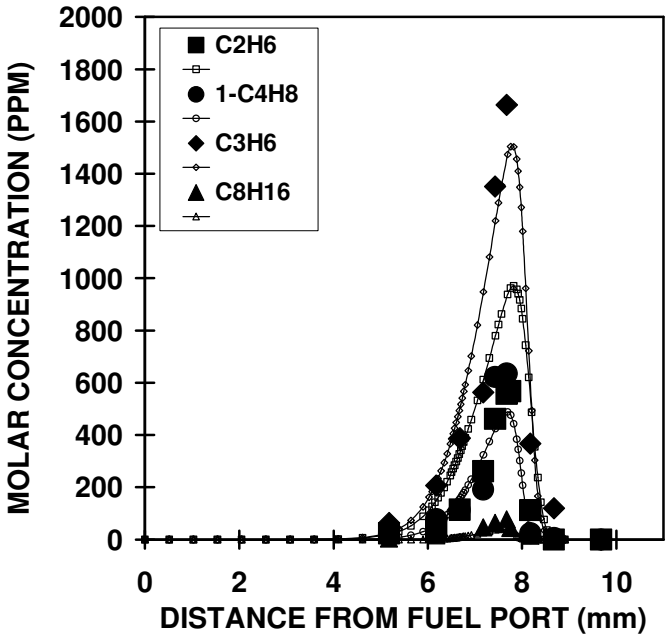

Figure 11: Experimental and computed species profiles obtained from the oxidation of MD in an atmospheric opposed-flow flame (1.8% MD, 42% O_2).

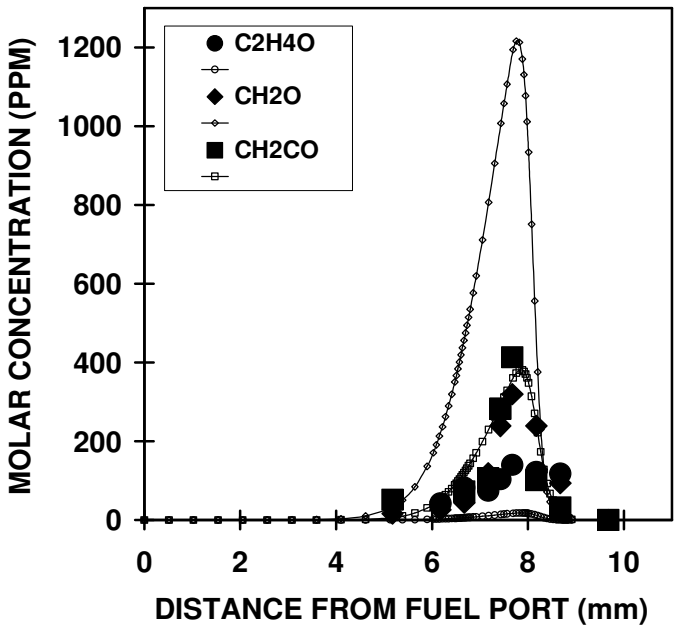

Figure 12: Experimental and computed species profiles obtained from the oxidation of MD in an atmospheric opposed-flow flame (1.8% MD, 42% O_2).

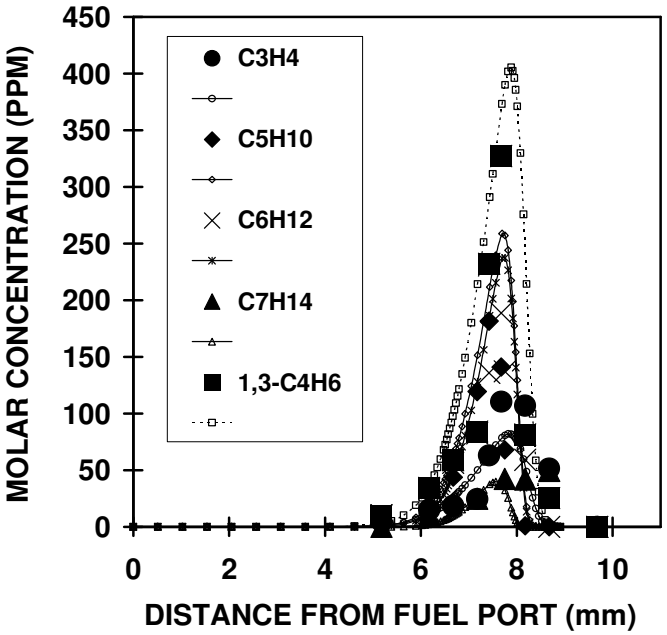

Figure 13: Experimental and computed species profiles obtained from the oxidation of MD in an atmospheric opposed-flow flame (1.8% MD, 42% O_2).

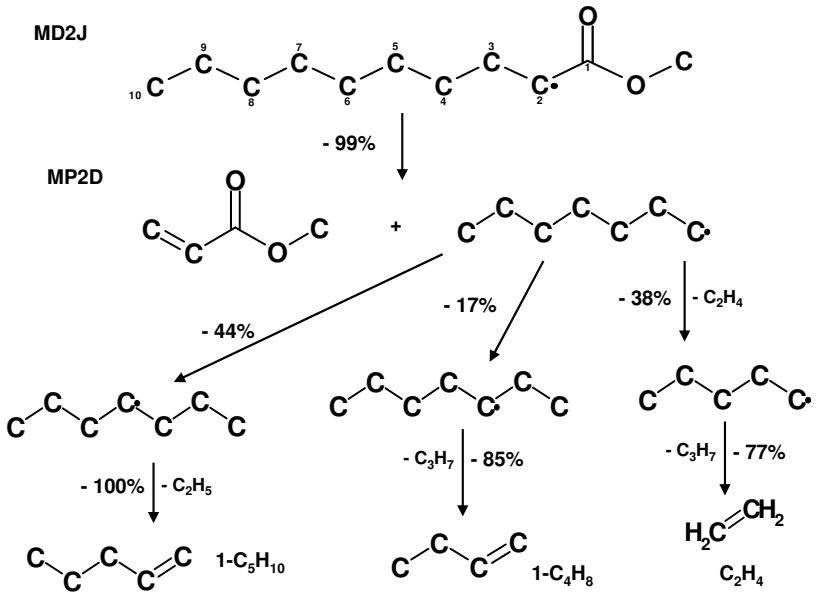

Figure 14: Reaction pathway diagram for consumption of the MD2J radical in the opposed-flow diffusion flame at T=1040 K.

Approximately 70% of the fuel is consumed via abstraction of H atoms from the #3 through #9 carbon atoms. An example of the subsequent reaction pathways is shown in Figure 15 for the MD4J radical. The radicals decompose via two routes, one leading to an alkene and a methyl ester radical, and the other forming an unsaturated methyl ester and an alkyl radical. The alkyl radicals eventually result in the formation of 1-alkenes. The model predicts that the unsaturated methyl esters are consumed mainly by unimolecular decomposition to form an allyl radical and a saturated methyl ester radical that is three carbon atoms shorter (e.g., methyl 6-heptenoate decomposes to the radical methyl $\dot{4}$-butanoate, methyl 7-octenoate decomposes to the radical methyl $\dot{4}$-pentanoate, etc.). These methyl ester radicals with the radical site on the terminal carbon undergo β-scission to form ethylene and smaller methyl ester radicals. The process continues until the radical site nears the carbonyl group and the radical decomposes to a low molecular weight oxygenated species.

Other radicals formed via abstraction of secondary H atoms from other carbons in the alkyl chain follow a similar path as MD4J. The radicals decompose via two routes, one leading to an alkene and a methyl ester radical, and the other forming an unsaturated methyl ester and an alkyl radical. The alkyl radicals eventually result in the formation of 1-alkenes, and as shown previously the concentration of 1-alkenes decreases with increasing carbon number. The model predicts that the unsaturated methyl esters are consumed mainly by unimolecular decomposition to form an allyl radical and a saturated methyl ester radical that is three carbon atoms shorter (e.g., methyl 6-heptenoate decomposes to the radical methyl $\dot{4}$-butanoate, methyl 7-octenoate decomposes to the radical methyl $\dot{4}$-pentanoate, etc.). These methyl ester radicals with the radical site on the terminal carbon undergo β-scission to form ethylene and smaller methyl ester radicals. The process continues until the radical site nears the carbonyl group and the radical decomposes to low a molecular weight oxygenated species.

5.3. Oxygenated Species

Table 2 presents the maximum predicted and measured mole fractions of several unsaturated methyl esters, aldehydes, enals, ketones, ketenes, and enols. The measured and predicted concentrations of oxygenated product species can add insight into the role of the ester moiety during combustion. The following is a discussion of several important oxygenated species and their chemistry in the flame.

The model performs well at predicting the maximum concentrations of ketene (CH_2CO), but overpredicts the maximum concentrations of formaldehyde (CH_2O) and underpredicts acetaldehyde + ethenol (C_2H_4O). This is the first time ketene concentrations have been measured in combustion studies of FAME. Figure 15 displays the primary pathway which forms 83% of the ketene in the flame at 1040 K; the methyl ester radical, ME2J, undergoes β-scission to form ketene and methoxy radical (CH_3O). Therefore, it is observed that the ester moiety contributes to the formation of ketene.

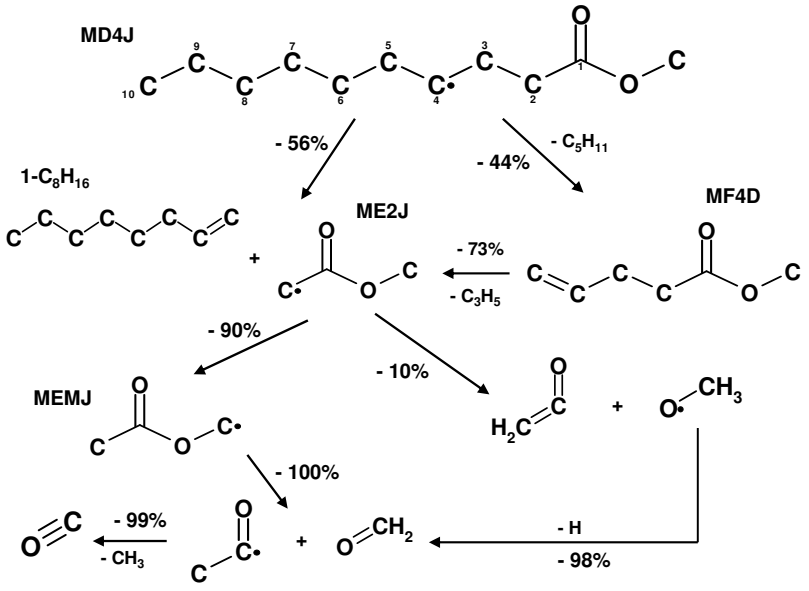

Figure 15: Reaction pathway diagram for consumption of the MD4J radical in the opposed-flow diffusion flame at T=1040 K.

The maximum predicted concentration of CH_2O is nearly 4 times greater than the measured concentration. This discrepancy can be attributed to either experimental errors or modeling inaccuracies, so both are discussed here. The experimental measurements for formaldehyde were performed using a GC/FID equipped with a methanizer. This method for detecting formaldehyde has yielded good results in JSR studies of FAME [2, 16, 22, 23]. However, extractive sampling measurements in flames [2, 16, 53, 54] have yielded similar discrepancies between measured and predicted formaldehyde, and it was suggested in [54] that formaldehyde may be lost due to polymerization in the sampling lines.

Approximately 86% of formaldehyde is formed via the decomposition of various methyl ester radicals with a radical on the methoxy site, such as MDMJ, MEMJ, and MP2DMJ. As shown in Figure 15 for MEMJ, these fuel radicals undergo β-scission to form formaldehyde. The current rate estimate for the decomposition of these radicals to formaldehyde are rough estimates, so detailed studies may reveal better rate constants.

The major discrepancy between the model and experiments is for unsaturated methyl ester species. The experiments did not measure detectable levels of any unsaturated methyl esters, but microliter injections of these unsaturated FAME verified that the analytical instrument used in this study was suitable for their detection. It should be noted that unsaturated methyl esters have been measured in other experimental studies of FAMEs [22–25, 55], albeit at low concentrations.

Methyl 2-propenoate (i.e., MP2D) is the unsaturated FAME predicted in the highest concentration.

Table 2: Maximum Measured and Predicted Concentration (PPM) of Oxygenated Species

	Measured	Predicted
Formaldehyde	319	1213
Ketene	413	381
Ethanal+Ethenol	100	33
Propanal	<LOD	<1
2-propenal	<LOD	32
2-propanone	<LOD	12
Methyl 2-propenoate	<LOD	939
Methyl 3-butenoate	<LOD	89
Methyl 4-pentenoate	<LOD	44
Methyl 5-hexenoate	<LOD	35

Figure 16 inidcates that 94% of the MP2D is formed via β-scission of various methyl ester radicals with a radical site on the α carbon (e.g., MD2J). High concentrations of methyl 2-propenoate are predicted because multiple pathways lead to various methyl ester radicals with a radical site on the α carbon, and these form methyl 2-propenoate faster than it can be consumed via H atom abstraction reactions. The rate parameters for the methyl 2-propenoate consumption have been determined based on analogies with saturated methyl ester molecules and unsaturated hydrocarbons. Fundamental rate studies may improve the predicted concentration of methyl 2-propenoate. Another explanation for the discrepancy between the model and predicted values is possible decomposition of methyl 2-propenoate upon contact with hot surfaces in the high pressure side of the sampling line. It is possible that FAME are reacting in the sampling line to form acetaldehyde+ethenol compounds which were measured in appreciable quantities, but not predicted to be significant by the model.

5.3.1. The Fate of the Ester Moiety

Previous studies on methyl butanoate combustion discussed the fate of the ester moiety at high temperatures. When applied to different experimental conditions (e.g., flames, premixed reactors, etc.), the MB models predict that the methoxycarbonyl radical is an important combustion intermediate. We ran the opposed-flow diffusion flame simulations for MB using the experimental conditions of Gail et al. [2] and the mechanism of Dooley et al. [4] to calculate how much of the fuel decomposes to form the methoxycarbonyl radical at high temperatures. The results indicate that approximately 23% of the fuel ends up in the methoxycarbonyl radical, as shown in Figure 17. The methoxycarbonyl radical primarily decays to form a methyl radical and CO_2. From a soot reduction standpoint this decarboxylation of the ester is not an

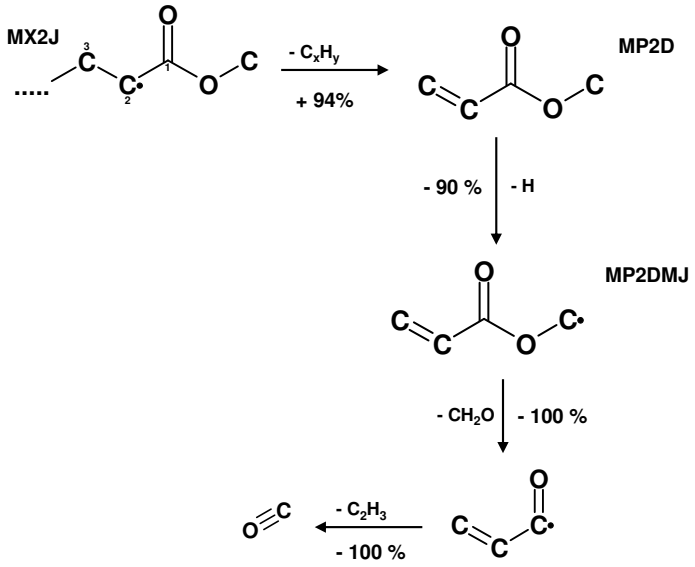

Figure 16: Reaction pathways for the formation and consumption of methyl 2-propenoate in the opposed-flow diffusion flame at T=1040 K.

efficient use of fuel-bound oxygen because two oxygen atoms are bonded to one carbon atom. It would be more efficient if the ester moiety led to the production of CO since each oxygen atom in the ester group would sequester one carbon atom from participating in the production of soot. Many researchers have hypothesized that the long chain FAME in biodiesel undergo similar reaction pathways as methyl butanoate, and therefore the ester moiety in biodiesel is not as efficient at supressing soot compared to other oxygenated moieties (e.g., aldehydes, ethers, alcohols, etc.). The present study on methyl decanoate offers additional insights to the aforementioned hypothesis.

The above analysis on MB indicates that the radical sites on the α and β carbons can lead to the methoxycarbonyl radical. At 1040 K, approximately 10% of MD is consumed via H-atom abstraction from the β carbon leading to the MD3J radical. This is much less than what was observed for methyl butanoate [2] under similar conditions, or even for methyl hexanoate in a JSR at 950 K [22]. Similarly, 19% of MD is consumed via H-atom abstraction from the α carbon whereas it is 27% for MB. These pathways in MD, and for longer chain FAME too, becomes less important because the number of H-atom abstraction sites increases with chain length. Furthermore, after abstraction from the β carbon, the resulting MD3J radical undergoes β-scission at equal rates to form either i. 1-nonene plus the methoxycarbonyl radical or ii. methyl 3-butenoate plus and a 1-hexyl radical. However, the analogous radical in MB (i.e., MB3J) strongly favours the route leading to the methoxycarbonyl radical, since β-scission forming methyl 3-butenoate is thermo-

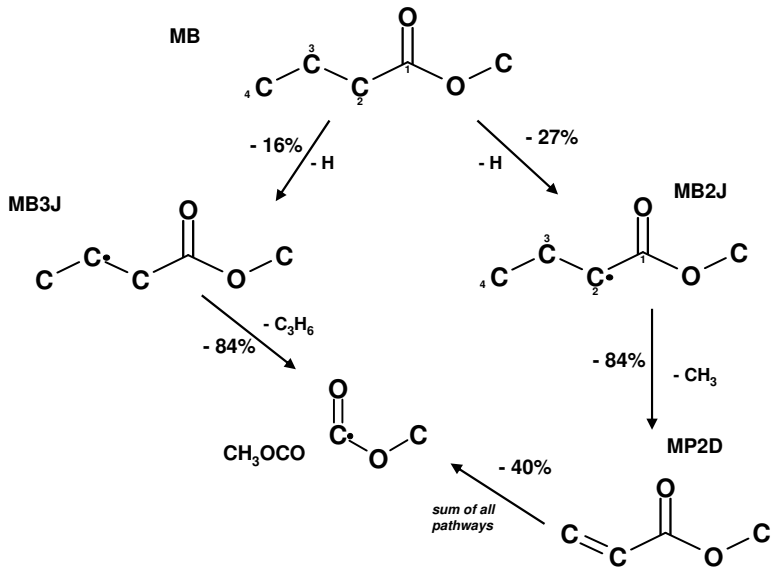

Figure 17: Reaction pathways leading to the formation of the methoxycarbonyl radical in the opposed-flow diffusion flame at T=1030 K given the experimental and modeling conditions of Gail et al. [2].

dynamically unfavourable for the MB3J radical. The importance of fuel radical isomerization reactions also become more important as the size of the FAME increases.

Similar to the previous studies on MB, the present MD mechanism predicts that the methoxycarbonyl radical decomposes to form CO_2. It is estimated that approximately 6% of the fuel ends up forming the CO_2 via the methoxycarbonyl radical, which is much lower than previous estimates based on MB (i.e., 23%). This number is expected to be even lower in longer chain FAME because of the increased number of potential pathways of fuel consumption.

It should be noted that the amount of fuel that ends up in the methoxycarbonyl radical depends on the experimental conditions (i.e., temperature, pressure, mixture fraction, etc.). The above analysis applies to high temperature oxidation where H-atom abstraction is predominant. Simulations should be conducted for conditions in which unimolecular decomposition is predominant for additional insights. In any case, this study suggests that decarboxylation of the ester group in long chain FAME is not significant. In fact, much of the original fuel bound oxygen leads directly to oxygenated species such as carbon monoxide, formaldehyde, and ketene, wherein one oxygen atom is bonded to one carbon atom. Therefore, the soot reducing efficiency of long chain FAME may be better than previously believed.

5.4. Jet Stirred Reactor

The proposed skeletal mechanism for MD was also validated against experimental JSR data for RME at ϕ=1.0, P=101.325 kPa, τ=1.0 s [26]. Since MD is a smaller molecule than RME, the inlet mole fraction

of MD was proportionally increased to match the inlet carbon flux of RME, as described by Herbinet et al. [28]. The comparison between the model predictions and experimental data is shown in Figures 18 and 19.

The skeletal mechanism performs similarly to the detailed MD mechanism [28]. The concentrations of CO_2, CO, C_2H_4, O_2, CH_4, and C_3H_6 are well predicted by the skeletal mechanism. However, the concentrations of 1-C_4H_8, 1-C_5H_{10}, and 1-C_6H_{12} are overpredicted by the model, which was also observed by Herbinet et al. [28]. The prediction of alkenes does not agree with measured values because RME consists of longer chain FAME with various degrees of unsaturation, while MD is fully saturated and has a smaller chain. Although there is no data available, RME is likely to have larger carbon chains leading to the formation of larger 1-alkenes (e.g., >C_8) than would MD; therefore, MD over predicts the concentrations of the smaller 1-alkenes (e.g., C_4-C_6).

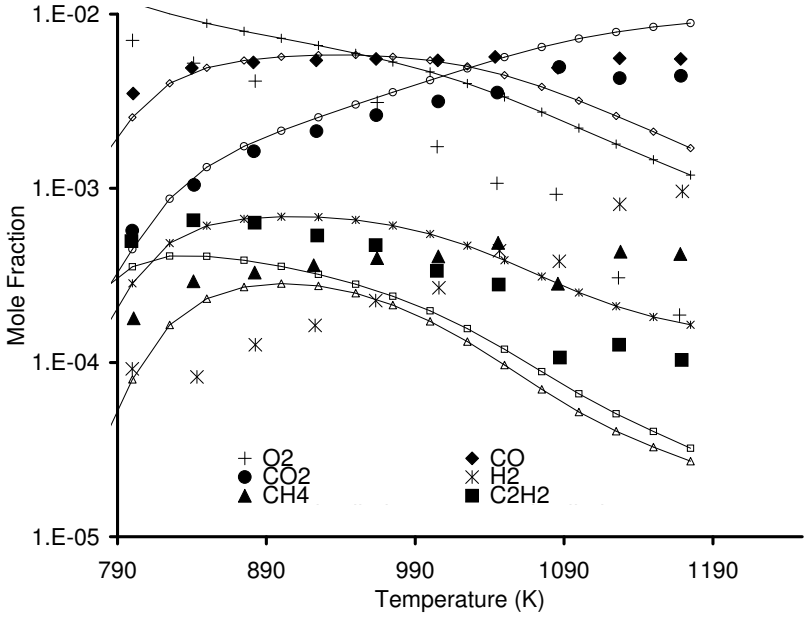

Figure 18: Comparison of proposed MD skeletal mechanism and experimental data for RME in a JSR at ϕ=1.0, P=101.325 kPa, τ=1.0 s [26].

6. Conclusions and Recommendations

This study is the first to present experimental data for methyl decanoate combustion that can be used for validating chemical kinetic mechanisms. The combustion of MD in the opposed-flow diffusion flame generates typical hydrocarbon combustion products (e.g., CO, CO_2, CH_4, C_2H_4, etc.). Of particular interest is the production of C_5-C_8 1-alkenes which are formed after β-scission of fuel radicals. The production of low molecular weight oxygenated compounds such as formaldehyde, ketene, and isomers of C_2H_4O is also

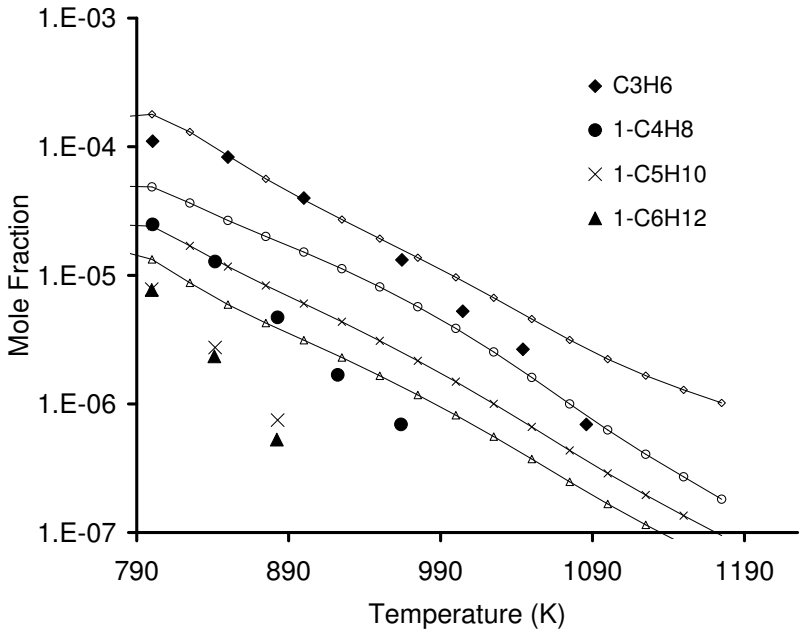

Figure 19: Comparison of proposed MD skeletal mechanism and experimental data for RME in a JSR at ϕ=1.0, P=101.325 kPa, τ=1.0 s [26].

observed.

The experimental data presented herein was used to validate an improved skeletal mechanism for the high temperature oxidation of MD. Initially, modifications were made to a previously proposed detailed mechanism for MD, and then an improved DRG algorithm was performed to create a skeletal mechanism. This new skeletal mechanism provides excellent qualitative prediction of experimentally measured species and temperature profiles in the MD opposed-flow diffusion flame. This study highlights the effectiveness of the DRG method in producing a mechanism that is computationally practical for one-dimensional flame simulations yet also retains a high level of chemical fidelity.

The proposed mechanism indicates that unsaturated methyl esters are an important intermediate in the combustion of saturated FAME. The present mechanism derives kinetic information for unsaturated methyl esters from analogous reaction pathways for alkenes. This approximation needs to be improved via fundamental studies on the thermochemical properties of unsaturated FAME. *Ab initio* calculations for unsaturated FAME will not only improve mechanisms for saturated FAME, but they will help build comprehensive mechanisms for unsaturated FAME, such as the one recently presented by Herbinet et al. for methyl decenoates [34]

7. Acknowledgements

The portion of this work supported by LLNL was performed under the auspices of the U.S. Department of Energy by Lawrence Livermore National Laboratory under Contract DE-AC52-07NA27344. The work at University of Connecticut was supported by the National Science Foundation under Grant No. OCI-0904771.

References

[1] E. Fisher, W. Pitz, H. Curran, C. Westbrook, Detailed chemical kinetic mechanisms for combustion of oxygenated fuels, Proc. Combust. Inst. 28 (2) (2000) 1579 – 1586.

[2] S. Gail, M. Thomson, S. Sarathy, S. Syed, A wide-ranging kinetic modeling study of methyl butanoate combustion, Proc. Combust. Inst. 31 (2007) 305–311.

[3] W. Schwartz, C. McEnally, L. Pfefferle, Decomposition and hydrocarbon growth processes for esters in non-premixed flames, J. Phys. Chem. A 110 (21) (2006) 6643–6648. doi:10.1021/jp0549576.

[4] S. Dooley, H. J. Curran, J. M. Simmie, Autoignition measurements and a validated kinetic model for the biodiesel surrogate, methyl butanoate, Combust. Flame 153 (1-2) (2008) 2–32. doi:10.1016/j.combustflame.2008.01.005.

[5] W. K. Metcalfe, S. Dooley, H. J. Curran, J. M. Simmie, A. M. El-Nahas, M. V. Navarro, Experimental and modeling study of C5H10O2 ethyl and methyl esters, J. Phys. Chem. A 111 (19) (2007) 4001–4014. doi:10.1021/jp067582c.

[6] S. M. Walton, M. S. Wooldridge, C. K. Westbrook, An experimental investigation of structural effects on the auto-ignition properties of two C-5 esters, Proc. Combust. Inst. 32 (Part 1) (2009) 255–262. doi:10.1016/j.proci.2008.06.208.

[7] A. Farooq, D. F. Davidson, R. K. Hanson, L. K. Huynh, A. Violi, An experimental and computational study of methyl ester decomposition pathways using shock tubes, Proc. Combust. Inst. 32 (Part 1) (2009) 247–253. doi:10.1016/j.proci.2008.06.084.

[8] L. K. Huynh, K. C. Lin, A. Violi, Kinetic modeling of methyl butanoate in shock tube, J. Phys. Chem. A 112 (51) (2008) 13470–13480. doi:10.1021/jp804358r.

[9] A. M. El-Nahas, M. V. Navarro, J. M. Simmie, J. W. Bozzelli, H. J. Curran, S. Dooley, W. Metcalfe, Enthalpies of formation, bond dissociation energies and reaction paths for the decomposition of model biofuels: Ethyl propanoate and methyl butanoate, J. Phys. Chem. A 111 (19) (2007) 3727–3739. doi:10.1021/jp067413s.

[10] A. Osmont, M. Yahyaoui, L. Catoire, I. Goekalp, M. T. Swihart, Thermochemistry of c-o, (co)-o, and (co)-c bond breaking in fatty acid methyl esters, Combust. Flame 155 (1-2) (2008) 334–342. doi:10.1016/j.combustflame.2008.06.007.

[11] A. Osmont, L. Catoire, I. Goekalp, M. T. Swihart, Thermochemistry of c-c and c-h bond breaking in fatty acid methyl esters, Energ. Fuel 21 (4) (2007) 2027–2032. doi:10.1021/ef070132e.

[12] A. Osmont, L. Catoire, I. Goekalp, Thermochemistry of methyl and ethyl esters from vegetable oils, Int. J. Chem. Kinet. 39 (9) (2007) 481–491. doi:10.1002/kin.20264.

[13] C. J. Hayes, D. R. Burgess, Jr., Exploring the oxidative decompositions of methyl esters: Methyl butanoate and methyl pentanoate as model compounds for biodiesel, Proc. Combust. Inst. 32 (Part 1) (2009) 263–270. doi:10.1016/j.proci.2008.05.075.

[14] L. K. Huynh, A. Violi, Thermal decomposition of methyl butanoate: Ab initio study of a biodiesel fuel surrogate, J. Org. Chem. 73 (1) (2008) 94–101. doi:10.1021/jo701824n.

[15] S. M. Sarathy, S. Gail, S. A. Syed, M. J. Thomson, P. Dagaut, A comparison of saturated and unsaturated C4 fatty acid methyl esters in an opposed flow diffusion flame and a jet stirred reactor, Proc. Combust. Inst. 31 (Part 1) (2007) 1015–1022. doi:10.1016/j.proci.2006.07.019.

[16] S. Gail, S. M. Sarathy, M. J. Thomson, P. Dievart, P. Dagaut, Experimental and chemical kinetic modeling study of small methyl esters oxidation: Methyl (e)-2-butenoate and methyl butanoate, Combust. Flame 155 (4) (2008) 635–650. doi:10.1016/j.combustflame.2008.04.007.

[17] W. K. Metcalfe, C. Togbe, P. Dagaut, H. J. Curran, J. M. Simmie, A jet-stirred reactor and kinetic modeling study of ethyl propanoate oxidation, Combust. Flame 156 (1) (2009) 250–260. doi:10.1016/j.combustflame.2008.09.007.

[18] T. Vaughn, Hammill, H. M., M., A. Marchese, Ignition delay of bio-ester fuel droplets, SAE Tech. Pap. Ser. 2006-01-3302.

[19] K. HadjAli, M. Crochet, G. Vanhove, M. Ribaucour, R. Minetti, A study of the low temperature autoignition of methyl esters, Proc. Combust. Inst. 32 (Part 1) (2009) 239–246. doi:10.1016/j.proci.2008.09.002.

[20] J. P. Szybist, J. McFarlane, B. G. Bunting, Comparison of simulated and experimental combustion of biodiesel blends in a single cylinder diesel hcci engine, SAE 2007 Trans.

[21] Y. Ra, R. D. Reitz, J. Mcfarlane, C. S. Daw, Development and validation of a reduced reaction mechanism for biodiesel fueled engine simulations, SAE 2008 Trans.

[22] G. Dayma, S. Gail, P. Dagaut, Experimental and kinetic modeling study of the oxidation of methyl hexanoate, Energ. Fuel 22 (3) (2008) 1469–1479. doi:10.1021/ef700695j.

[23] G. Dayma, C. Togbe, P. Dagaut, Detailed kinetic mechanism for the oxidation of vegetable oil methyl esters: New evidence from methyl heptanoate, Energ. Fuel 23 (2009) 4254–4268. doi:10.1021/af000184y.

[24] Y. Zhang, A. L. Boehman, Experimental study of the autoignition of C8H16O2 ethyl and methyl esters in a motored engine@articleISI:000264756800151, author = Dworkin, S. B. and Schaffer, A. M. and Connelly, B. C. and Long, M. B. and Smooke, M. D. and Puccio, M. A. and McAndrew, B. and Miller, J. H., title = Measurements and calculations of formaldehyde concentrations in a methane/N-2/air, non-premixed flame: Implications for heat release rate, journal = PROCEEDINGS OF THE COMBUSTION INSTITUTE, year = 2009, volume = 32, pages = 1311-1318, number = Part 1, abstract = A non-sooting, lifted, methane/air, coflowing, non-premixed flame has been studied experimentally and computationally. The flame structure was computed by solving the fully elliptic governing equations, utilizing a 35 species chemical kinetic mechanism, detailed transport coefficients and ail optically thin radiation submodel. Gas temperature, major species mole fractions, and non-fuel hydrocarbon concentrations were experimentally mapped in two dimensions with both probe techniques (coupled to infrared absorption spectroscopy and on-line mass spectrometry) and in situ optical diagnostics (laser-induced fluorescence, Rayleigh and Raman scattering). Contour plots of measured and computed formaldehyde concentrations and fluorescence signals agree well and both revealed a region of intense formaldehyde production near the lifted flame base. High formaldehyde production rates correlated well with regions of high heat release. Further, regions of the dominant formaldehyde formation reaction, CH3 + O = HCHO + H, also correlated with areas of maximum heat release rate. (C) 2009 The Combustion Institute. Published by Elsevier Inc. All rights reserved., address = 360 PARK AVE SOUTH, NEW YORK, NY 10010-1710 USA, affiliation = Miller, JH (Reprint Author), George Washington Univ, Dept Chem, 725 21st St NW,Room 107, Washington, DC 20052 USA. [Puccio, M. A.; McAndrew, B.; Miller, J. H.] George Washington Univ, Dept Chem, Washington, DC 20052 USA. [Dworkin, S. B.; Schaffer, A. M.; Connelly, B. C.; Long, M. B.; Smooke, M. D.] Yale Univ, Dept Mech Engn, New Haven, CT 06520 USA., author-email = houston@gwu.edu, doc-delivery-number = 427CG, doi = 10.1016/j.proci.2008.05.083, funding-acknowledgement = NSF [NSF-CTS 0330230, CTS-0328296]; DoE [DE-FG02-88ER13966]; NASA [NAG9-01480, NNC04AA03A], funding-text = The authors thank the NSF (Grants NSF-CTS 0330230 and CTS-0328296), DoE (Grant DE-FG02-88ER13966) and NASA (Grants NAG9-01480 and NNC04AA03A) for their generous financial support. The authors also thank Dr. Rui Yang who led the IC laser development team at the Jet Propulsion Laboratory., issn = 1540-7489, journal-iso = Proc. Combust. Inst., keywords = Formaldehyde concentrations; Methane/air diffusion flame; Heat release rates, keywords-plus = LOCAL RECTANGULAR REFINEMENT; MODIFIED NEWTON METHOD; DIFFUSION FLAMES; DIODE-LASER; FLUORESCENCE; SOOT, language = English, number-of-cited-references = 37, publisher = ELSEVIER SCIENCE INC,

subject-category = Thermodynamics; Energ. Fuel; Engineering, Chemical; Engineering, Mechanical, times-cited = 1, type = Article, unique-id = ISI:000264756800151 , Combust. Flame (2009) doi:10.1016/j.combustflame.2009.09.003.

[25] Y. Zhang, Y. Yang, A. L. Boehman, Premixed ignition behavior of C9 fatty acid esters: A motored engine study, Combust. Flame 156 (6) (2009) 1202–1213. doi:10.1016/j.combustflame.2009.01.024.

[26] P. Dagaut, S. Gail, M. Sahasrabudhe, Rapeseed oil methyl ester oxidation over extended ranges of pressure, temperature, and equivalence ratio: Experimental and modeling kinetic study, Proc. Combust. Inst. 31 (Part 2) (2007) 2955–2961. doi:10.1016/j.proci.2006.07.142.

[27] J. P. Szybist, A. L. Boehman, D. C. Haworth, H. Koga, Premixed ignition behavior of alternative diesel fuel-relevant compounds in a motored engine experiment, Combust. Flame 149 (1-2) (2007) 112–128. doi:10.1016/j.combustflame.2006.12.011.

[28] O. Herbinet, W. J. Pitz, C. K. Westbrook, Detailed chemical kinetic oxidation mechanism for a biodiesel surrogate, Combust. Flame 154 (3) (2008) 507–528. doi:10.1016/j.combustflame.2008.03.003.

[29] T. Lu, C. K. Law, Toward accommodating realistic fuel chemistry in large-scale computations, Prog. Energ. Combust. 35 (2) (2009) 192–215. doi:10.1016/j.pecs.2008.10.002.

[30] K. Seshadri, T. Lu, O. Herbinet, S. B. Humer, U. Niemann, W. J. Pitz, R. Seiser, C. K. Law, Experimental and kinetic modeling study of extinction and ignition of methyl decanoate in laminar non-premixed flows, Proc. Combust. Inst. 32 (Part 1) (2009) 1067–1074. doi:10.1016/j.proci.2008.06.215.

[31] S. M. Sarathy, M. J. Thomson, C. Togbe, P. Dagaut, F. Halter, C. Mounaim-Rousselle, An experimental and kinetic modeling study of n-butanol combustion, Combust. Flame 156 (4) (2009) 852–864. doi:10.1016/j.combustflame.2008.11.019.

[32] C. McEnally, U. Koylu, L. Pfefferle, D. Rosner, Soot volume fraction and temperature measurements in laminar non-premixed flames using thermocouples, Combust. Flame 109 (4) (1997) 701–720.

[33] R. J. K. et al., Chemkin pro (2009).

[34] O. Herbinet, W. J. Pitz, C. K. Westbrook, Detailed chemical kinetic oxidation mechanism for a biodiesel surrogate, Combust. Flame accepted October 2009. In Press. (3). doi:10.1016/j.combustflame.2008.03.003.

[35] H. Curran, Rate constant estimation for C1 to C4 alkyl and alkoxyl radical decomposition, Int. J. Chem. Kinet. 38 (4) (2006) 250–275. doi:10.1002/kin.20153.

[36] D. Healy, H. J. Curran, J. M. Simmie, D. M. Kalitan, C. M. Zinner, A. B. Barrett, E. L. Petersen, G. Bourque, Methane/ethane/propane mixture oxidation at high pressures and at high, intermediate and low temperatures, Combust. Flame 155 (2008) 441–448.

[37] C. K. Westbrook, W. J. Pitz, O. Herbinet, H. J. Curran, E. J. Silke, A comprehensive detailed chemical kinetic reaction mechanism for combustion of n-alkane hydrocarbons from n-octane to n-hexadecane, Combust. Flame 156 (1) (2009) 181–199. doi:10.1016/j.combustflame.2008.07.014.

[38] P. Dagaut, M. Reuillon, M. Cathonnet, D. Voisin, High-pressure oxidation of normal-decemberane and kerosene in dilute conditions from low to high-temperature, J. Chim. Phys. PCB. 92 (1) (1995) 47–76.

[39] T. Lu, C. Law, A directed relation graph method for mechanism reduction, Proc. Combust. Inst. 30 (2005) 1333–1341.

[40] T. Lu, C. Law, On the applicability of directed relation graph to the reduction of reaction mechanisms, Combust. Flame 146 (2006) 472–483, 2006.

[41] E. R. Ritter, J. W. Bozzelli, THERM: Thermodynamic property estimation for gas phase radicals and molecule, Int. J. Chem. Kinet. 23 (1991) 767–778.

[42] S. Benson, Thermochemical Kinetics, 2nd edition, Wiley, New York, 1976.

[43] R. Sumathi, W. H. G. Jr., Oxygenate, oxyalkyl and alkoxycarbonyl thermochemistry and rates for hydrogen abstraction from oxygenates, Physical Chemistry Chemical Physics 5 (2003) 3402–3417.

[44] L. Tee, S. Gotoh, W. Stewart, Molecular parameters for normal fluids - lennard-jones 12-6 potential, Ind. Eng. Chem.

Fund. 5 (3) (1966) 356.

[45] H. Wang, M. Frenklach, Transport properties of polycyclic aromatic hydrocarbons for flame modeling, Combust. Flame 96 (1-2) (1994) 163–170.

[46] P. Linstrom, W. Mallard, NIST chemistry webbook, NIST standard reference database number 69 (2005). URL http://webbook.nist.gov

[47] A. McClellan, Tables of Experimental Dipole Moments, Freeman, San Francisco, 1963.

[48] S. Bohm, O. Exner, Prediction of molecular dipole moments from bond moments: testing of the method by DFT calculations on isolated molecules, Physical Chemistry Chemical Physics 6 (3) (2004) 510–514. doi:10.1039/b312595p.

[49] D. R. Lide (Ed.), CRC Handbook of Chemistry and Physics, 87th Edition, Taylor and Francis, Boca Raton, FL, 2007. URL http:/www.hbcpnetbase.com

[50] R. Bosque, J. Sales, Polarizabilities of solvents from the chemical composition, J. Chem. Inf. Comp. Sci. 42 (5) (2002) 1154–1163. doi:10.1021/ci025528x.

[51] J. M. Simmie, H. J. Curran, Energy barriers for the addition of h, CH3, and C2H5 to CH2=CHX [X = H, CH3, OH] and for h-atom addition to RCH=O [R = H, CH3, C2H5, n-C3H7]: Implications for the gas-phase chemistry of enols, J. Phys. Chem. A 113 (27) (2009) 7834–7845. doi:10.1021/jp903244r.

[52] G. Black, H. Curran, S. Pichon, J. Simmie, V. Zhukov, Bio-butanol: Combustion properties and detailed chemical kinetic model, Combust. Flame in press (2009) doi:10.1016/j.combustflame.2009.07.007.

[53] S. B. Dworkin, A. M. Schaffer, B. C. Connelly, M. B. Long, M. D. Smooke, M. A. Puccio, B. McAndrew, J. H. Miller, Measurements and calculations of formaldehyde concentrations in a methane/n-2/air, non-premixed flame: Implications for heat release rate, Proc. Combust. Inst. 32 (Part 1) (2009) 1311–1318. doi:10.1016/j.proci.2008.05.083.

[54] M. S. Kurman, R. H. Natelson, N. P. Cernansky, D. L. Miller, Preignition oxidation chemistry of the major jp-8 surrogate component: n-dodecane, American Institute of Aeronautics and Astronautics (2009) 1–19.

[55] M. H. Hakka, P.-A. Glaude, O. Herbinet, F. Battin-Leclerc, Experimental study of the oxidation of large surrogates for diesel and biodiesel fuels, COMBUSTION AND FLAME 156 (11) (2009) 2129–2144. doi:10.1016/j.combustflame.2009.06.003.